International Communications in Heat and Mass Transfer 145 (2023) 106844

Contents lists available at ScienceDirect

International Communications in Heat and Mass Transfer

journal homepage: www.elsevier.com/locate/ichmt

An unsteady flow through porous media leads to a Newtonian fluid presence of CNTS and suction/injection

U.S. Mahabaleshwar [a], K.N. Sneha [a], L.M. Pérez [b], O. Manca [c,*]

[a] Department of Studies in Mathematics, Davangere University, Shivagangothri, Davangere 577 007, India
[b] Departamento de Física, FACI, Universidad de Tarapacá, Casilla 7D, Arica, Chile
[c] Dipartimento di Ingegneria, Università degli Studi della Campania Luigi Vanvitelli, Aversa, CE, Italy

ARTICLE INFO

Keywords:
Darcy model
CNT
Radiation
Stagnation point
Heat transfer
Biot number

ABSTRACT

An action of CNTs flow access an unstable motion of a Newtonian fluid past a stagnation point on a stretched sheet using a penetrable medium is investigated in this paper. Once the fluid commences circulating with the flow of time, it flows. Flow is influenced by heat exchange with the surroundings. The implicitly limited component method is employed to track an unstable system of non-dimensional PDE with an associated boundary layer. Approaches, along with the relevant barrier circumstances, are acquired analytically. An influence of mass transpiration, volume fraction, and thermal radiation is investigated on Newtonian fluid flow using the penetrable medium. Heat transmission in a liquid with electrical conductivity, including heat source /sink across a continually stretched /shrinking surface with a Biot number. The importance of the present exertion is the stream of carbon nanotubes owing to Darcy porous media using linear heat radiation and an analytical approach. The nanoparticles provide important properties in enhancing the heat exchange procedure as well as thoroughly achieved applications in industry. It is discovered that the basic resemblance models accept two-phase for both extending /contracting sheets. In presence of calculation upon momentum with temperature jump conditions is accessible plots aimed at varying predictions of certain physical properties. Analyzing the properties of Darcy porous media of heat transport in the presence of radiation from a flat surface, the problem is solved analytically using incomplete gamma functions. Depending on the kind of boundary heating, the analytical equation for temperature is obtained in terms of power series.

1. Introduction

In the latest days, the flow has become increasingly crucial. Simply a few applications are petroleum transport, treatment of wastewater, ignition, and nuclear plant pipes. Moreover, because raw oil is extracted via reservoir pore spaces, the flow pattern across porous materials has become an essential factor. Such examinations reveal their applications due to a broad range of scientific as well as configuration systems, especially in the emulsification polymer expulsion, the boundary layer outwards to substance behavior conveyors, the aerodynamic expulsion of glass puffing, paper production, and plastic sheets, as well as the boundary layer beside a liquid layer in the decomposition method.

Two criteria would essentially influence the appropriate liquid mechanical characteristics as a result of such a mechanism: the refrigerating liquid developed. Since flow and heat transmission can be regulated independently, liquids exhibiting non-Newtonian characteristics that are electronically directed can be employed as conditioning liquids. The quantity of stretching is essential, as faster lengthening results in crystallization. Sakiadis [1] examined the motion of the barrier layer due to a persistent, thick layer affecting it with a steady velocity. Crane [2] interest was extended to a stretched surface, as well as a particular exact-form solution. Following that, a few researchers [3–6] generalized the flow problem being prolonged in several dimensions, leading to a number of references. Adding nanoscale materials to refrigerants is one technique to improve their thermal performance. Besides, the nanoparticles are known as a combination of nanoscale fragments that have disseminated more heat as a result of their superior thermal efficiency, consequently improving component heat transfer rates. The cooling of hot surfaces in various forms is among the nanofluid applications. The cooling effects of nanofluid on a heated plate were compared to the effects of a base fluid [7–10].

Nanofluids across a stretching sheet with cross-diffusion impacts on hydromagnetic fields were investigated by Reddy and Chamkha [11].

* Corresponding author at: Dipartimento di Ingegneria, Università degli Studi della Campania Luigi Vanvitelli, Via Roma 29, 81031 Aversa, CE, Italy.
E-mail addresses: u.s.m@davangereuniversity.ac.in (U.S. Mahabaleshwar), lperez@academicos.uta.cl (L.M. Pérez), oronzio.manca@unicampania.it (O. Manca).

https://doi.org/10.1016/j.icheatmasstransfer.2023.106844

Available online 18 May 2023
0735-1933/

Nomenclature

Symbols	Descriptions (S. I. units)
Bi	Biot number $(-)$
Da^{-1}	Darcy number $(-)$
d	stretching/shrinking constant (s^{-1})
$f(\eta)$	transverse velocity $(-)$
$f_\eta(\eta)$	axial velocity $(-)$
$F(\eta)$	$f(\eta)+\eta$transverse velocity $(-)$
$G(t,x)$	integration constant $(-)$
K	permeability $(-)$
k^*	coefficient of mean absorption (m^{-2})
N_R	radiation parameter $(-)$
P	pressure (Nm^{-2})
Pr	Prandtl number $(-)$
q_r	heat flux (Wm^{-2})
T	temperature (K)
t	time (s)
U_w	velocity at wall (ms^{-1})
U_∞	unsteady free stream velocity (ms^{-1})
(u,v)	velocity components of x and y axis (ms^{-1})
V_w	velocity of wall transpiration (ms^{-1})
V_c	mass transpiration $(-)$

Greek symbols

α	solution domain $(-)$
β	parameter of unsteadiness $(-)$
λ	stretching/shrinking sheet $(-)$
μ	dynamic viscosity $(Kgm^{-1}\,s^{-1})$
ν	kinematic viscosity (m^2s^{-1})
$\theta(\eta)$	temperature profile $(-)$
κ	thermal conductivity (m^2s^{-1})
σ^*	Stefan-Boltzmann constant $(Wm^{-2}\,K^{-4})$
ρ	density (Kgm^{-3})
ε_1 to ε_4	nanofluid parameters $(-)$
Γ	incomplete gamma function $(-)$

Subscripts

f	base fluid $(-)$
nf	nanofluid $(-)$

Abbreviations

BCs	boundary conditions $(-)$
BBL	backward boundary layer $(-)$
CNTs	carbon nanotubes $(-)$
FBL	forward boundary layer flow $(-)$
MWCNTs	multiwall CNTs $(-)$
ODE	ordinary differential equation $(-)$
PDE	partial differential equation $(-)$
SWCNTs	single wall CNTs $(-)$

Natural convection past a nonisothermal, vertically porous medium saturated with nanofluid is investigated by Gorla and Chamkha [12]. Iijima [13] discovered carbon nanotubes, a material composed of carbon nanotube atoms and oxy carbons. The applications of single-walled nanotubes and multi-walled nanotubes in industry and medicine are gaining popularity due to their direct effects on increasing the thermal conductivity of base fluids. Since heat transfer fluids used in power generation, microelectronics cooling, chemical processing, refrigeration, air conditioning, transportation, and an assortment of other applications have low thermal conductivity, it is essential to increase their effective thermal conductivity to improve heat transfer rate [14,15]. In an experimental study on the convective heat transfer properties of CNT nanofluids, dependent on a secondary refrigerant in a tubular heat exchanger, Kumaresan et al. [16] With CNTs, Liu and Liang [17] created another type of watery drag-reducing fluid. This has the dual impact of reducing drag and improving heat transfer.

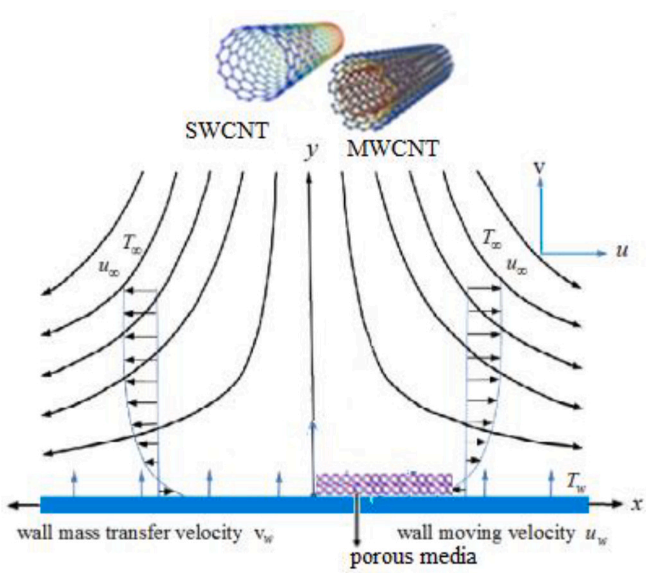

Fig. 1. Schematic representation of flow problem.

The results of many physical and analytical types of research on the heat transmission of nanofluid are discussed. Nanofluids are discussed as a method for improving the thermodynamic capacity of solar detectors. The MWCNT nanofluid with the mass fraction is explored physically in a flat plate solar extractor connected to a hemispherical cavity transmitter. Ahmadi et al. [18–20]. Because of these possibilities, the impact of mass transfer and energy properties concerning the air stream and water surface is examined by Gu et al. [21]. The thermal conductivity and dynamic viscosity of a hybrid nanofluid were calculated by Esfe et al. [22].

Mahabaleshwar et al. [23–25] extended the sheet through heat transfer within sight of radiation and heat source/sink effects over the stretching sheet and subsequently. Further, Mahabaleshwar et al. [26,27] published an article on the MHD flow with carbon nanotubes and the effect of mass transpiration and radiation on it. Effective viscosity is the dynamic viscosity that is associated with the Brinkman term. The magnitude of the viscosity ratio has been studied in the past with differing results. M Mastroberardino et al. [28] The Darcy-Brinkman condition's validity has additionally been explored, especially when it derives liquid in relation to the boundary layer examined by Nield [29]. Slip flow of Jeffrey nanofluid with activation energy and entropy generation applications examined by Jile et al. [35]. Some researchers studied about the Modeling MHD stagnation point flow of thixotropic fluid with non-uniform heat absorption/generation and New modeling and analytical solution of fourth grade (non-Newtonian) fluid by a stretchable magnetized Riga devic, the effect of magnetic field on rotating stretched disk flow with heat transfer. Here stuied about the study of Newtonian heating in flow of hybrid nanofluid (SWCNTs + CuO + Ethylene glycol) past a curved surface with viscous dissipation and Mixed convective slip flow of hybrid nanofluid (MWCNTs + Cu + Water), nanofluid (MWCNTs + Water) and base fluid (Water): a comparative investigation [36–42].

Table 1
Proposed nanofluid models. [43].

Nanofluid models	
Nanofluid proprieties	Relative expression
$\rho_{nf} = (1-\phi)\rho_f + \phi\,\rho_{CNT}$	$\rho_r = \frac{\rho_{nf}}{\rho_f} = (1-\phi) + \phi\,\frac{\rho_{CNT}}{\rho_f}$
$\mu_{nf} = \frac{\mu_f}{(1-\phi)^{2.5}}$	$\mu_r = \frac{\mu_{nf}}{\mu_f} = \frac{1}{(1-\phi)^{2.5}}$
$(\rho C_p)_{nf} = (1-\phi)(\rho C_p)_f + \phi(\rho C_p)_{CNT}$	$(\rho C_p)_r = \frac{(\rho C_p)_{nf}}{(\rho C_p)_f} = (1-\phi) + \phi\frac{(\rho C_p)_{CNT}}{(\rho C_p)_f}$
$k_{nf} = \left[\frac{(1-\phi)+2\phi\left(\frac{k_{CNT}}{k_{CNT}-k_f}\right)ln\left(\frac{k_{CNT}+k_f}{2k_f}\right)}{(1-\phi)+2\phi\left(\frac{k_f}{k_{CNT}-k_f}\right)ln\left(\frac{k_{CNT}+k_f}{2k_f}\right)}\right]k_f$	$k_r = \frac{k_{nf}}{k_f} = \frac{(1-\phi)+2\phi\left(\frac{k_{CNT}}{k_{CNT}-k_f}\right)ln\left(\frac{k_{CNT}+k_f}{2k_f}\right)}{(1-\phi)+2\phi\left(\frac{k_f}{k_{CNT}-k_f}\right)ln\left(\frac{k_{CNT}+k_f}{2k_f}\right)}$

Table 2
Properties of each phase. Mahabaleshwar et al. [44], Sneha et al. [45].

Properties	*SWCNT*	*MWCNT*	H_2O
$\rho(kgm^{-3})$	425	796	997
$C_P\left(Jkg^{-1}K^{-1}\right)$	2600	1600	4179
$k(Wm^{-1}K^{-1})$	6.600	3.000	0.613
$\mu(\times 10^{-5}Pas)$	–	–	

The novelty of this analysis is to explore the properties of carbon nanotubes due to a Darcy permeable medium using non-uniform thermal radiation using a hypothesized convergence analytical approach. Because of the query's nonlinear and unstructured nature, a successful resolution is unique. As a result, the proposed method is given an analytical description. Nonlinear ODEs are created from the controlling PDEs. As a result, the current examination will delve deeper into the computable correlations between wall impacts and the Darcy porous media. This equation is solved analytically and then expressed as an energy equation in the form of an incomplete gamma function. We defined several parameters here, including the Biot number, Darcy porous medium, radiation parameter, and mass transpiration. These results can be examined by using dual solutions for the upper and lower branches. A collection of comparable coefficients among the elements of motion, just definite extents, is considered for appraising the association among flow as well as temperature. The details are defined by expanding tables and graphs.

2. Physical formulation and solutions

The consequence of a permeable stretching/shrinking surface on the unstable flow as well as heat transport of CNTs with radiation is considered. By using a CNT with porous media, the 2-dimensional components (x, y) are delineated in Fig. 1. In this velocity boundary layer, we add SWCNT and MWCNT to improve the thermophysical properties of the nanofluid. (See Tables 1 and 2.)

The governing equation in vector form is given by

$$\nabla.\vec{q} = 0 \tag{A}$$

$$\rho_{nf}\left(\vec{q}_t + (\vec{q}.\nabla)\vec{q}\right) = -\nabla p + \mu_{nf}\nabla^2\vec{q} - \frac{\mu_{nf}}{k}\vec{q}, \tag{B}$$

$$(\rho C_P)_{nf}\left(\vec{q}_t + (\vec{q}.\nabla)T\right) = k_{nf}\left(\nabla^2 T\right) - \frac{\partial q_r}{\partial y}. \tag{C}$$

The succeeding formula is employed to compute the unsteady flow stream velocity quite far distant from the surface.

$$U_\infty = -\frac{dx}{1-at}, \tag{1}$$

here constant denotes, $d > 0$stretching surface, $d < 0$ shrinking surface, a is the constant. Consider wall velocities of motion are$U_w$with V_w respectively, and hence, the average absorption velocity is considered. Following is the computation of the external free stream velocity at the barrier.

$$U_w = \frac{\lambda dx}{1-at}, \tag{2}$$

where λrepresents the constant, $\lambda > 0$ sustaining flow, if $\lambda < 0$, be in conflict with the flow, $\lambda = 0$, Falkner-Skan flows are converted, where $\lambda = -\frac{U_w}{U_\infty}$, $V_w(x,t)$ is the y-direction transpiration velocity**.**

The transformed governing equation of Eq. (A) to (C) interms of fundamental equations of continuity, momentum, and temperature is as follows Fang et al. [46].

$$\frac{\partial u}{\partial x} + \frac{\partial v}{\partial y} = 0, \tag{3}$$

$$\rho_{nf}\left(\frac{\partial u}{\partial t} + u\frac{\partial u}{\partial x} + v\frac{\partial u}{\partial y}\right) = -\frac{\partial P}{\partial x} + \mu_{nf}\left(\frac{\partial^2 u}{\partial x^2} + \frac{\partial^2 u}{\partial y^2}\right) - \frac{\mu_{nf}}{k}u, \tag{4}$$

$$\rho_{nf}\left(\frac{\partial v}{\partial t} + u\frac{\partial v}{\partial x} + v\frac{\partial v}{\partial y}\right) = -\frac{\partial P}{\partial y} + \mu_{nf}\left(\frac{\partial^2 v}{\partial x^2} + \frac{\partial^2 v}{\partial y^2}\right), \tag{5}$$

$$(\rho C_P)_{nf}\left(\frac{\partial T}{\partial t} + u\frac{\partial T}{\partial x} + v\frac{\partial T}{\partial y}\right) = k_{nf}\left(\frac{\partial^2 T}{\partial x^2} + \frac{\partial^2 T}{\partial y^2}\right) - \frac{\partial q_r}{\partial y}. \tag{6}$$

Where the imposed B·Cs are as follows:

$$u(x,0,t) = \frac{\lambda dx}{1-at}, \quad v(x,0,t) = V_w(x,t), \quad -K_f T_y = h(T_w - T_\infty) \quad \text{at } y = 0,$$
$$u(x,\infty,t) = -\frac{dx}{1-at}, \quad T \to T_\infty \quad \text{as } y \to \infty. \tag{7}$$

The flow is divided into two kinds: FBL and BBL depending on the selection of the porous stretching/shrinking velocity component d. FBL refers to the increase in flow caused by sheets released through the slit and travelling towards positive infinity, while BBL refers to persistent stretching from positive infinity and approaching the slit. The boundary layers of this category exhibit various physical characteristics that have important implications for manufacturing and technical activities.

Afterward, we introduced the non-dimensional variables. (See [47])

$$\psi(x,y,t) = xd\sqrt{\frac{\nu_f}{1-at}}f(\eta), \quad \theta(\eta) = \frac{(T-T_w)}{(T_w - T_\infty)}, \quad \eta = yd\sqrt{\frac{1}{\nu_f(1-at)}}. \tag{8a}$$

Non-dimensional variables are employed to obtain velocity components as below.

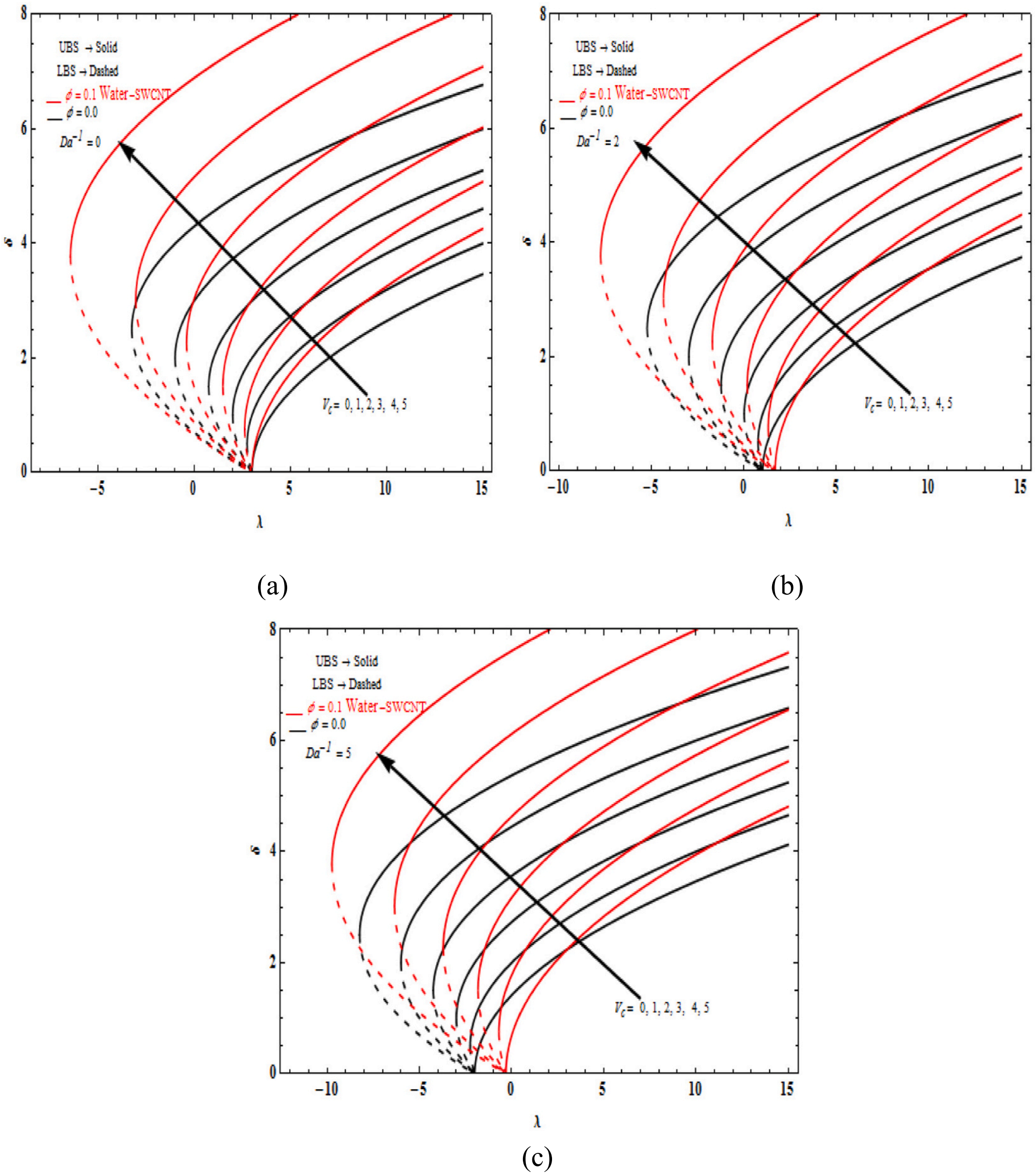

Fig. 2. An effect of δaginst λwall moving constraint for altered values of the $V_c$with (a) $Da^{-1}=0$ (b) $Da^{-1}=2$ (c)$Da^{-1}=5$.

$$u=\frac{dx}{1-at}f_\eta(\eta),v=-\sqrt{\frac{\nu_f}{1-at}}df(\eta). \tag{8b}$$

So as consequence, the rate at which wall transpiration is $v_w(x,0,t)=\sqrt{\frac{\nu_f}{1-at}}df(0)$.

Using the Rosseland approximation [30], radiative heat flux is described as

$$q_r=-\frac{4\sigma^*}{3k^*}\frac{\partial T^4}{\partial y}, \tag{9}$$

In which σ^* is known as Stefan-Boltzman constant as well as $k^*$is the coeeficient of mean absorption. The hypothesis is that temperature modification is conveyed as a linear purpose in the fourth power of temperature. The existing Taylor's series extension of the duration T∞ with the value T4 as follows. Assumedly, the temperature variations inside the flow are negligibly small, allowing $T^4$to be represented as a linear function of temperature:

$$T^4=T_\infty^4+4T_\infty^4(T-T_\infty)+6T_\infty^2(T-T_\infty)^2+\dots\dots.. \tag{10}$$

After negleting the higher order terms of the Eq. (10), we have

$$T^4\cong 3T_\infty^4+4T_\infty^3T \tag{11}$$

Through expending Eqs. (9), (10) and (11), Eq. (3) moderates to

$$uT_x+vT_y=\frac{\kappa_f}{(\rho C_P)_{nf}}\left(\frac{\kappa_{nf}}{\kappa_f}+\frac{16\sigma^*T_\infty^3}{3k^*\kappa_f}\right)T_{yy}. \tag{12}$$

2.1. Pressure gradient solution

The benefits observe $\frac{\partial P}{\partial y}$ differential pressure gradient, is the result of t with y, is estimated with based on the velocity components as well as Eq. (4), and is governed via x. notably, $\frac{\partial P}{\partial y}=F(t,y)$ and $P=\int F(t,y)dy+G(t,x)$, where $G(t,x)$ stands for the integrating factor. $\frac{\partial P}{\partial x}=\frac{\partial G(t,x)}{\partial x}$, it would be apart from y with retains equally in the flow field as well as the barrier layer, could be deduced. Determine the x- velocity of the flow field using $u=U_\infty$ with $\frac{\partial p}{\partial x}$.

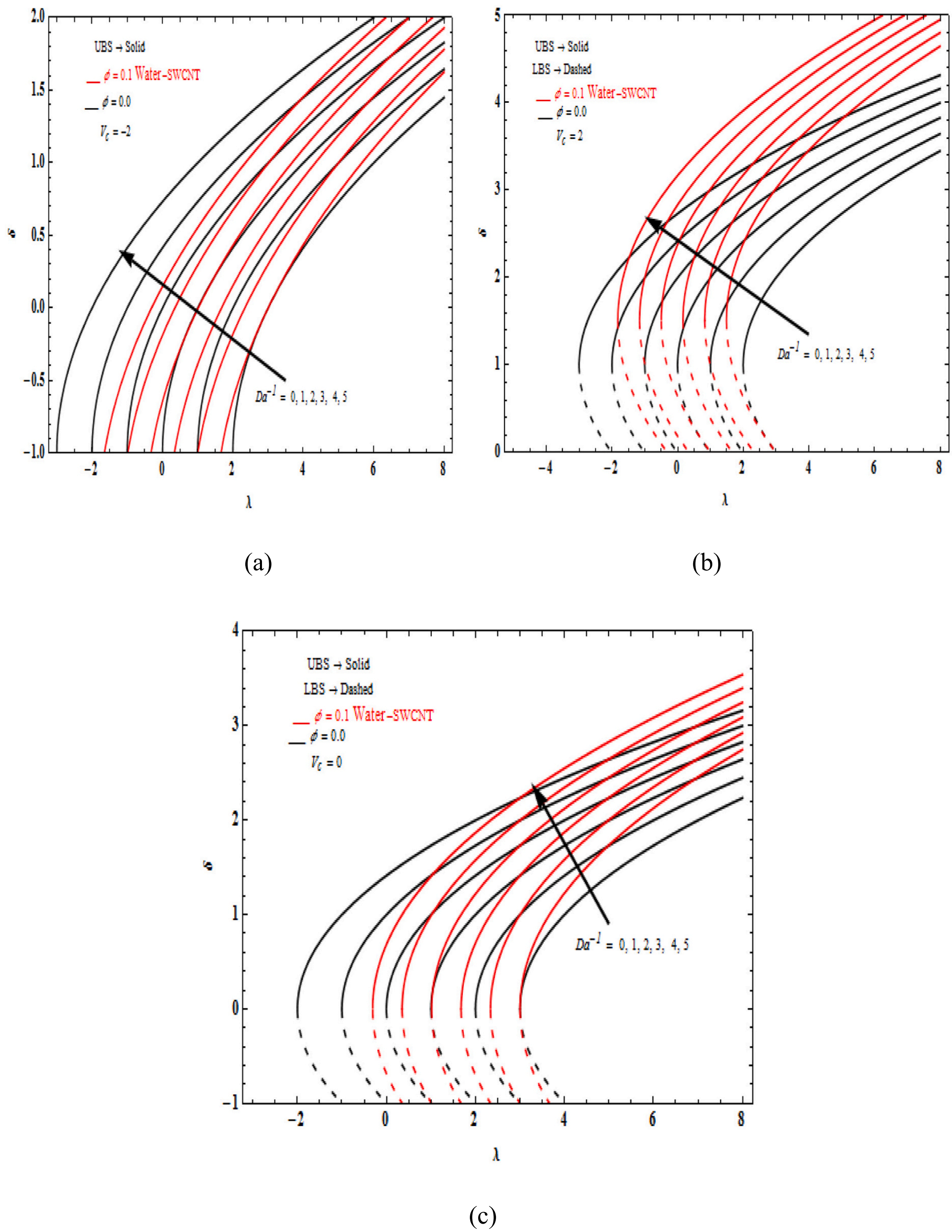

Fig. 3. Effect of δversus λwall moving constraint for altered values of Da^{-1} with (a) $V_c = 2$ (b) $V_c = -2$ (c)$V_c = 0$.

$$-\frac{1}{\rho}\frac{\partial P}{\partial x} = (1-\beta)\frac{\varepsilon_2 d^2 x}{(1-at)^2}, \tag{13}$$

The property of velocity acceleration and deceleration is represented through β, here $\beta = \frac{a}{d}$ is the unsteadiness factor. although $\beta > 0$, accelerating surface velocities,$\beta < 0$, wall decelerating, $\beta = 0$ steady state, $p_0$is integration constant.

$$\frac{1}{\rho_f}(P_0 - P) = \frac{\varepsilon_2}{2}(1-\beta)\frac{d^2x^2}{(1-at)^2} + \varepsilon_2\int\frac{\partial v}{\partial t}dy + \varepsilon_2\frac{v^2}{2} - \varepsilon_1\nu_f\frac{\partial v}{\partial y}, \tag{14}$$

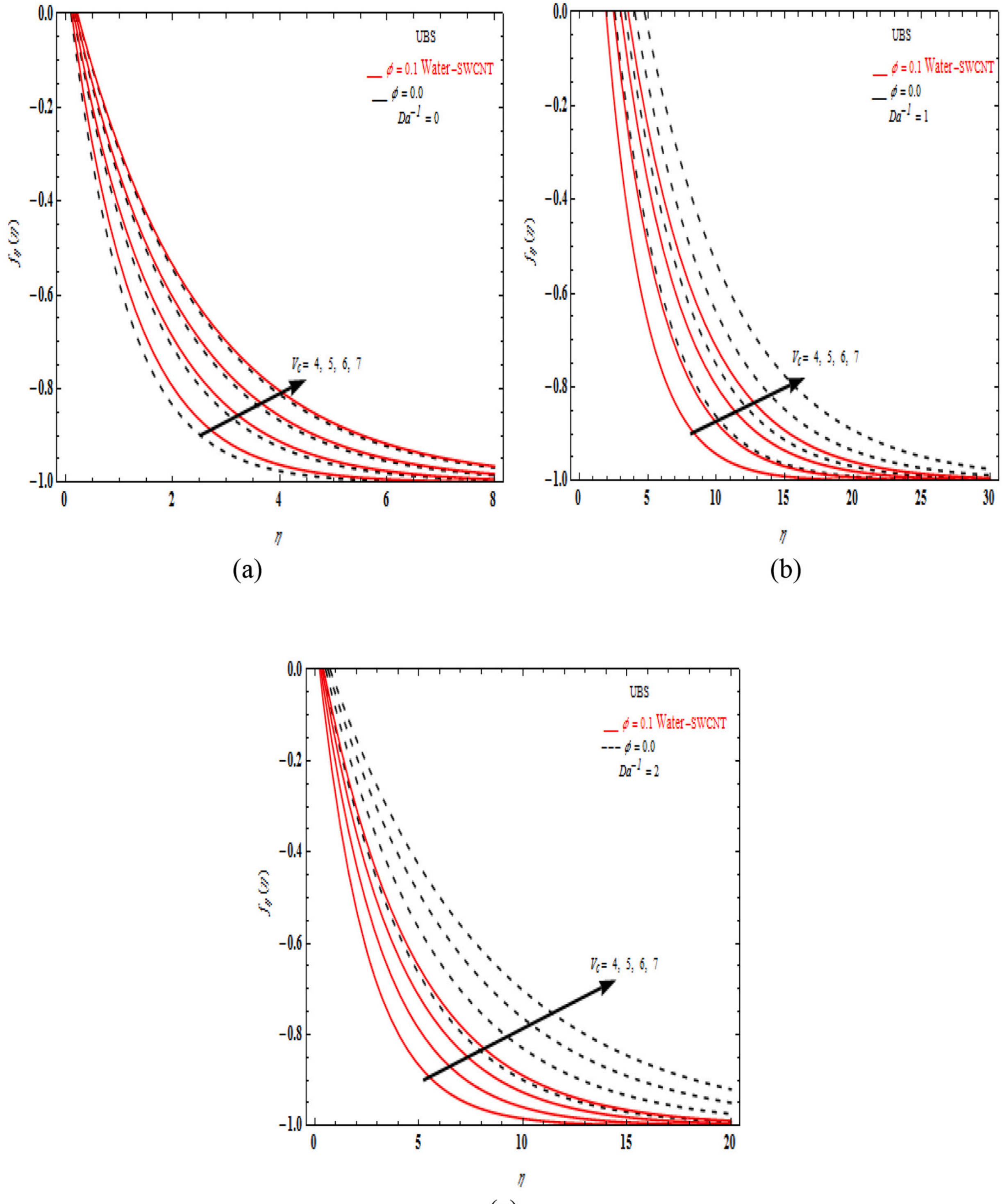

Fig. 4. Influence of $f_\eta(\eta)$ versus η for altered values of mass transpiration with (a) $Da^{-1} = 0$ (b) $Da^{-1} = 1$ (c)$Da^{-1} = 2$.

2.2. Momentum and energy equation solution

Eq. (3) is satisfied identically by using Eq. (8a), and Eq. (5)–(6) which takes the form of an ODEs

$$\varepsilon_1 \frac{d^3 f}{d\eta^3} + \varepsilon_2 \left[f \frac{d^2 f}{d\eta^2} - \left(\frac{df}{d\eta}\right)^2 + 1 - \beta\left(\frac{df}{d\eta} + \frac{1}{2}\eta \frac{d^2 f}{d\eta^2} - 1\right)\right] - \varepsilon_1 Da^{-1}\left(1 + \frac{df}{d\eta}\right) = 0, \tag{15}$$

$$(\varepsilon_4 + N_R)\frac{d^2\theta}{d\eta^2} + \varepsilon_3 Pr\left(f - \frac{\beta\eta}{2}\right)\frac{df}{d\eta} = 0. \tag{16}$$

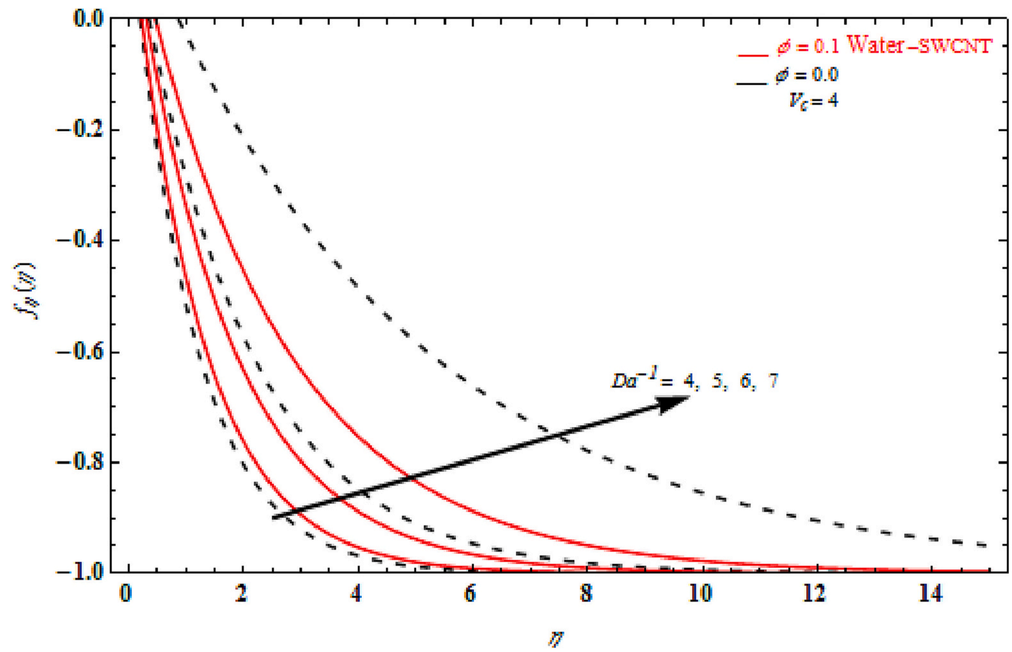

Fig. 5. Impact of axial velocity versus similarity variable for altered values of Da^{-1} with $V_c = 4$.

An imposed barrier constraints are

$$\left(\frac{df}{d\eta}\right)(0) = \lambda, f(0) = V_C, \quad \left(\frac{df}{d\eta}\right)(\infty) = -1, \\ \left(\frac{d\theta}{d\eta}\right)(0) = -Bi(1-\theta(0)), \qquad \theta(\infty)\rightarrow 0. \tag{17}$$

Where, the various physical parameters are as follows;

$$\varepsilon_1 = \frac{\mu_{nf}}{\mu_f}, \varepsilon_2 = \frac{\rho_{nf}}{\rho_f}, \varepsilon_3 = \frac{(\rho C_P)_{nf}}{(\rho C_P)_f}, \varepsilon_4 = \frac{k_{nf}}{k_f},$$

is $Pr = \frac{\nu_f}{\alpha_f}$, Prandtl number, $Da^{-1} = \frac{\mu_f}{K\rho_f d}$, Darcy number, $N_R = \frac{16\sigma^* T_\infty{}^3}{3k^* \kappa_f}$, Thermal radiation, $\lambda = -\frac{U_w}{U_\infty}$, $\lambda > 0$ stretching sheet $\lambda < 0$ is shrinking sheet parameters.

When $Da^{-1} = N_R = 0$, the consequences are transformed into Fang et al. [31]. $Da^{-1} = 0$, the data is then transformed into Xenos et al. [32]. The current findings are transformed into Mahabaleshwar et al. [33], who established the non-existence of a method for $\beta = 2$, and may be generalized either to positive β. As a result, the method takes into account the precise parameter of β. For a decelerating liquid flow with $\beta = 2$, the analytical solution for conservation eq. (15) is obtained. The ODEs that result are as described under the prescribed constraints $\frac{df}{d\eta}(0) = f(0) = 0$, $\frac{df}{d\eta}(\infty) = 1$, transformed into Hiemenz [34] outcomes in the 1st feature $\varepsilon_1 \frac{d^3f}{d\eta^3} + \varepsilon_2\left[f\frac{d^2f}{d\eta^2} - \frac{df^2}{d\eta} + 1\right] = 0$ in the eq. (15). For this condition, $\beta\left(\frac{df}{d\eta} + \frac{1}{2}\eta\frac{d^2f}{d\eta^2} + 1\right)$ is an unsteady influence, and the resistance to the flow over a porous medium is $\varepsilon_1 Da^{-1}\left(1 + \frac{df}{d\eta}\right)$, respectively. The momentum equation can be computed using, a further resemblance criterion $F(\eta) = f(\eta) + \eta$ being incorporated into the system, moreover succeeding in regulating equations is,

$$\varepsilon_1\frac{d^3F}{d\eta^3} + \varepsilon_2\left(F\frac{d^2F}{d\eta^2} + 4\frac{dF}{d\eta} - \left(\frac{dF}{d\eta}\right)^2\right) - \varepsilon_1 Da^{-1}\frac{dF}{d\eta} = 0. \tag{18}$$

Although, the aforementioned regulating BCs are modified to

$$F(0) = V_c, \quad \left(\frac{dF}{d\eta}\right)(0) = \lambda + 1, \ \text{ at } \eta = 0, \\ \left(\frac{dF}{d\eta}\right)(\infty) = 0, \qquad \text{as } \eta\rightarrow\infty. \tag{19}$$

The mandatory restriction in Eq. (19) advised that $F = p + q[exp(-\alpha\eta)]$ being recommended, along α being a constant estimated through Eq. (19). Depending on the prescribed analytical pattern for Eq. [18], it is thought that the required solution should revolve around the pattern together with associated BCs (19) and the aforesaid choice of $\frac{dF}{d\eta}$, since this approach $F = p + q[exp(-\alpha\eta)]$ putting in BCs, Lets find a solution $p + q = V_c$, $q = -\frac{(\lambda+1)}{\alpha}$ as well as

$$F(\eta) = V_C + \frac{\lambda+1}{\alpha}[1 - exp(-\alpha\eta)], \tag{20}$$

On applying prescribed solution Eq. (20) to Eq. (18) in order to get the exponent α worth as,

$$\varepsilon_1\alpha^2 - \varepsilon_2 p\alpha + 4\varepsilon_2 - \varepsilon_1 Da^{-1} = 0, \tag{21}$$

$$\alpha = \frac{\varepsilon_2 V_C \pm \sqrt{(\varepsilon_2 V_C)^2 + 4\varepsilon_1\left(\varepsilon_2\lambda + \varepsilon_1 Da^{-1} - 3\varepsilon_1\right)}}{2\varepsilon_1}, \tag{21a}$$

The fundamental problem is presupposed by

$$f(\eta) = -\eta + V_c + \frac{\lambda+1}{\alpha}[1 - exp(-\alpha\eta)] \tag{22}$$

2.3. Energy equation

Now recommend a new component ξ which obeys the correlation coefficients to identify the precise solution of temperature Eq. (12).

$$\xi = (1+\lambda)\frac{Pr}{\alpha^2}e^{-\alpha\eta}. \tag{23}$$

Putting $F(\eta)$ as well as Eq. (23) in Eq. (12) proceeds the following

$$(\varepsilon_4 + N_r)\,\xi\frac{\partial^2\theta}{\partial\xi^2} + \left((\varepsilon_4 + N_R) - \varepsilon_3 Pr\left(1 + \frac{4\varepsilon_2 + \varepsilon_1 Da^{-1}}{\alpha^2}\right) + \varepsilon_3\xi\right)\frac{\partial\theta}{\partial\xi} = 0, \tag{24}$$

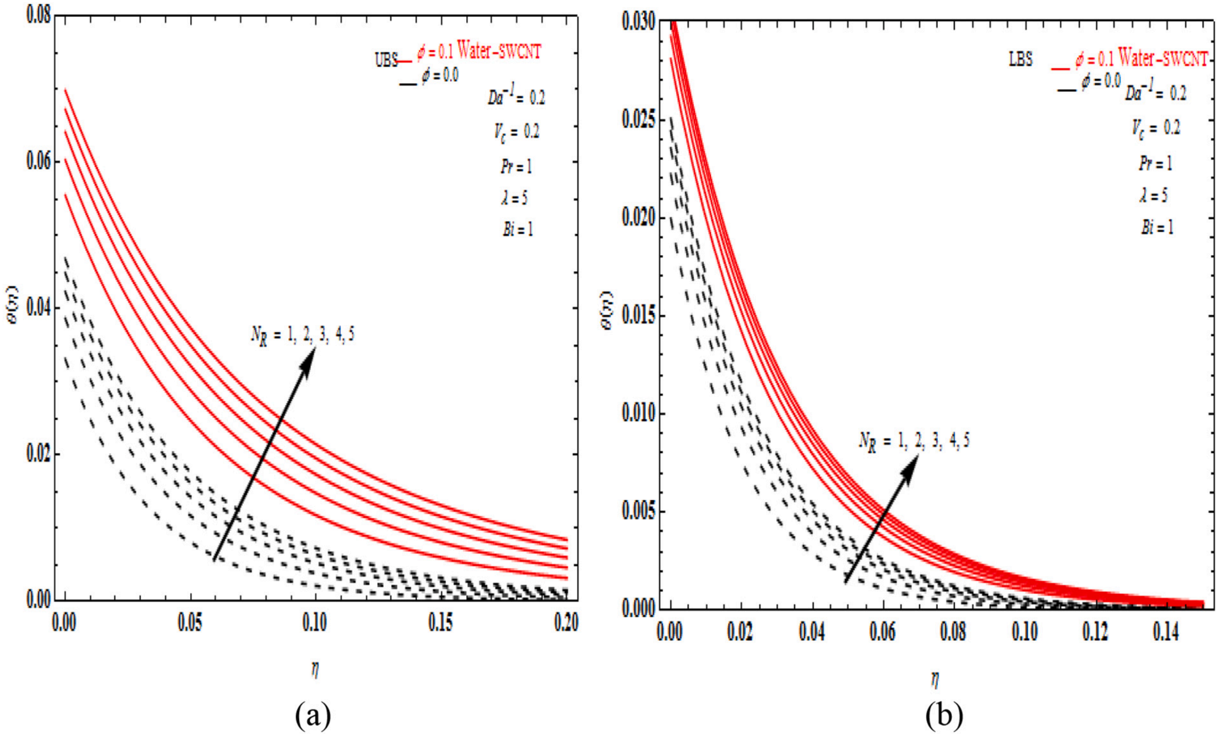

Fig. 6. An impact of$\theta(\eta)$ upon η for different values of $N_R$with (a) UBS (b) LBS.

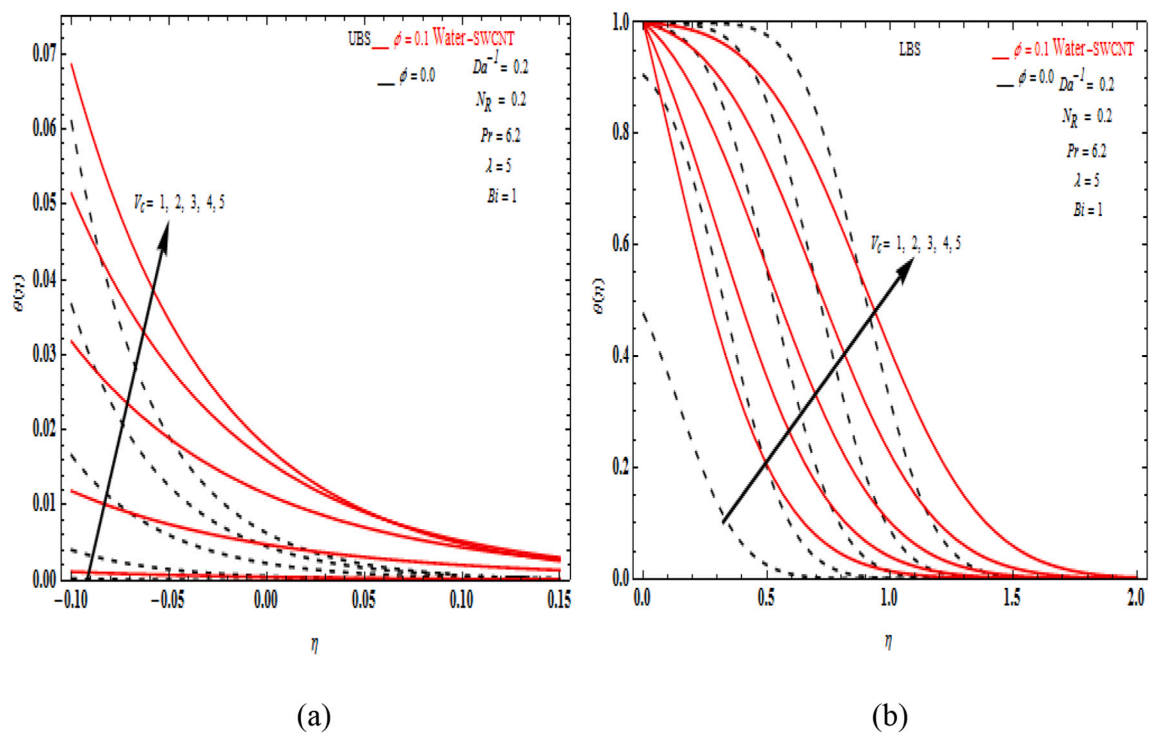

Fig. 7. An impact of$\theta(\eta)$ upon η for different values of $V_c$with (a) UBS (b) LBS.

The B. Cs reduces to

$$(1+\lambda)\frac{Pr}{\alpha}\theta_\eta\left((1+\lambda)\frac{Pr}{\alpha^2}\right) = Bi\left(1-\theta\left((1+\lambda)\frac{Pr}{\alpha^2}\right)\right), \theta(0)\rightarrow 0. \tag{25}$$

the pivotal point of the transformation (23) be $\xi = 0$. Due to this, Frobenius technique is employed to analyse the power solutions of Eq. (24)

$$\theta(\xi) = \sum_{r=0}^{\infty} a_r \xi^{n+r}. \tag{26}$$

Afterwards derivatives of the first as well as 2nd order Eq. (26) with respect to ξ with using the aforementioned in combination $\frac{\partial\theta}{\partial\eta}$ as well as $\frac{\partial^2\theta}{\partial\eta^2}$ terms, Eq.(24) specified as

$$\xi(\varepsilon_4+N_r)\sum_{r=0}^{\infty}(n+r)(n+r-1)a_r\xi^{n+r-2}+\left((\varepsilon_4+N_r)-\varepsilon_3 Pr\left(1+\frac{4}{\alpha^2}\right)+\varepsilon_3\xi\right)\sum_{r=0}^{\infty}(n+r)a_r\xi^{n+r-1}=0 \tag{27}$$

When the recurrence relation is used in connection with the ensuing values of $n=0, n=1-\frac{k_1}{k_2}$ respectively

$$a_r=-\frac{\varepsilon_3(n+r-1)}{(n+r)[c_2(n+r-1)+c_1]}a_{r-1}. \tag{28}$$

$$\theta(\eta)=\frac{Bi\Gamma\left(1-\frac{k_1}{k_2},0\right)-Bi\Gamma\left(1-\frac{k_1}{k_2},-(\lambda+1)\varepsilon_3\frac{Pr}{\alpha^2}e^{-\alpha\eta}\right)}{\left\{\alpha\left(-(\lambda+1)\varepsilon_3\frac{Pr}{\alpha^2}\right)^{1-\frac{k_1}{k_2}}exp\left((\lambda+1)\varepsilon_3\frac{Pr}{\alpha^2}\right)+Bi\Gamma\left(1-\frac{k_1}{k_2},0\right)-Bi\Gamma\left(1-\frac{k_1}{k_2},-(\lambda+1)\varepsilon_3\frac{Pr}{\alpha^2}\right)\right\}}. \tag{30}$$

here

$$k_2=(\varepsilon_4+N_r), \text{with } \ k_1=(\varepsilon_4+N_r)-\varepsilon_3 Pr\left(1+\frac{4\varepsilon_2+\varepsilon_1 Da^{-1}}{\alpha^2}\right),$$

In order to solve Eq. (27), employing this recurrence relation as well as the components of n, is modified as below.

$$\theta(\xi)=C_1C_0+C_2C_0\left(1-\frac{k_1}{k_2}\right)(-\varepsilon_3)^{-\left(1-\frac{k_1}{k_2}\right)}\left[\Gamma\left(1-\frac{k_1}{k_2},0\right)-\Gamma\left(1-\frac{k_1}{k_2},-\xi\varepsilon_3\right)\right]. \tag{29}$$

Finding the values of C_1 and C_2we get

$C_1=0,$

$$C_2=\frac{Bi}{c_0\left(1-\frac{k_1}{k_2}\right)(-\varepsilon_3)^{\frac{k_1}{k_2}-1}}\left\{\alpha\left(-(\lambda+1)\varepsilon_3\frac{Pr}{\alpha^2}\right)^{1-\frac{k_1}{k_2}}exp\left((\lambda+1)\varepsilon_3\frac{Pr}{\alpha^2}\right)+Bi\Gamma\left(1-\frac{k_1}{k_2},0\right)-Bi\Gamma\left(1-\frac{k_1}{k_2},-(\lambda+1)\varepsilon_3\frac{Pr}{\alpha^2}\right)\right\}^{-1}.$$

With inserting, the conjecture in terms of is establishedC_1 as well as C_2 quantities to Eq. (29) incomplete gamma function described as

3. Results and discussion

The current analytical issue takes into account an unstable laminar flow of Darcy porous media along CNTs, the presence of mass transpiration as well as thermal radiation. While translating PDEs to ODEs via similarity transformations, the analytical findings can be derived and stated as an incomplete gamma function. An exact consequences being momentum, as well as energy patterns graphs are depicted, since they show impacts of converse Darcy numberDa^{-1}, thermal radiationN_R, stretching/shrinking constraint, and different components. Moreover, most of the contemporary illustrations portray a correlation of momentum of single as well as multivalued CNTs amdist strong volume fraction $\phi=0.1$ and $\phi=0.0$ here dotted lines represent lower branch solution, with solid lines express upper branch solution.

Fig. 2a-c shows an impactof the $V_c$on the fluid flow on the stretching/shrinking surface. The solution domain is depicted in these images as a

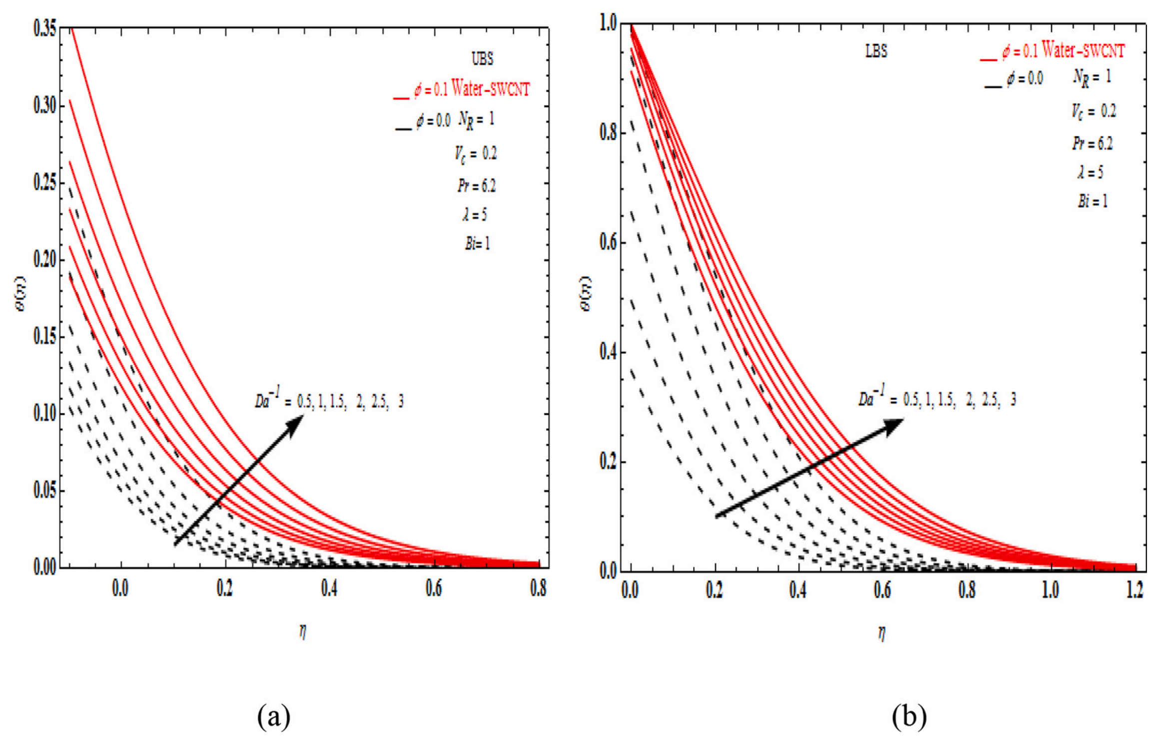

Fig. 8. An impact of$\theta(\eta)$ upon η for different values of $Da^{-1}$with (a) UBS (b) LBS.

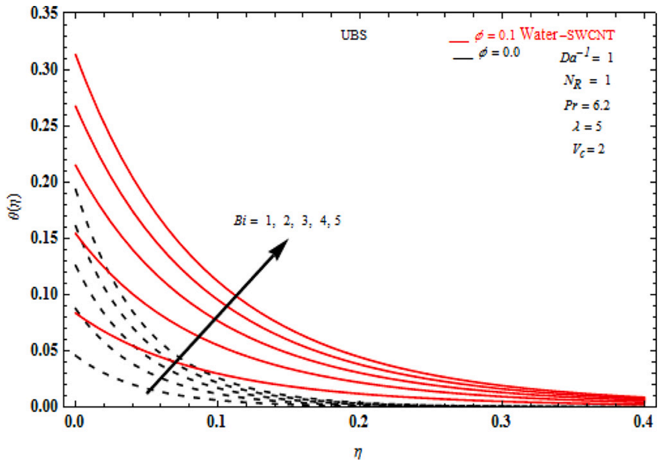

Fig. 9. Impact of$\theta(\eta)$ on η for altered values of $Bi$with UBS.

plot of δin expressions of $\lambda$by maintaining V_c while changing the other. There is a dual nature behavior here, with $\delta > 0$ for the UBS signified by a solid and $\delta < 0$for LBS signified by a dotted line, respectively. The formation of the solution is investigated with inverse Darcy number in the current results, and the occurrence of inverse Darcy number has a considerable effect on the dual solution. The present result, when $V_c$increases, causes $\delta$to rise while λdecreases. The nanofluids are efficiency in the laminar domain at high shear rate as the boundary layer rises. The performance of nanofluids is affected by both the drop in particle volume fraction and the increase in the flow pattern.

Fig. 3a-c depicts the influence of δon λ for several values ofDa^{-1}. In this case, δrises as Da^{-1}rises and λdeclines. Solid lines signify upper branch solution, with dashed lines signify lower branch solution. Here, black solid lines denote the $\phi = 0.0$ as well as Red solid lines suggest $\phi = 0.1$, for instance of no permeability, suction, as well as injection cases, respectively.

Figs. 4 and 5 show the consequence of mass transpiration V_c, Da^{-1} upon $f_\eta(\eta)$againstη, correspondingly, in order to stretched scenarios. An increase in mass transpiration$V_c$givresults in a proportional enhances in $f_\eta(\eta)$ as displayed in the Fig. 4a-c. it's illustrious that when the value of $f_\eta(\eta)$ rises, the width of the barrier layer enhances in addition. Also at simultaneously $\phi = 0.1$ generates a slightly greater $f_\eta(\eta)$ pattern apart from those of $\phi = 0.0$, as the inverse Darcy number increases, the solid volume fraction $\phi = 0.0$ increases more than that of$\phi = 0.1$. Fig. 5. It can be seen that when the inverse Darcy number does upwards shift the $f_\eta(\eta)$ profile slope, there is hidde difference between both $\phi = 0.0$ as well as $\phi = 0.1$. While Darcy number rises, viscous effects will be less important, and so velocity defects in the fluid flow will propagate less as expected. In reality, while stretching a sheet, the force and influence of the boundary condition is more important than the fluid's. An increase in the size of the mass transpiration parameter leads in a comparable decreases in the axial velocity profiles in both porous stretching and shrinking instances. The boundary layer thins as a result of mass transpiration in the stretching/shrinking sheet. As a result, a full examination of all of their effects will be exhaustive, requiring a massive amount of computing to be evaluated analytically for various parameter combinations. As a consequence, given the following parameters is stretching/shrinking parameter, mass transpiration, and porous parameter. Because of their physical features, the nanoparticles disrupted fluid.

Figs. 6,7,8, and 9 show the impact of thermal radiation parameters N_R, mass transpiration V_c, Darcy number Da^{-1}on the temperature distribution in Biot number cases when it is possible to use mass suction to stretch and contract limits. Due to the value of N_r enhanced $\theta(\eta)$ is reduced in the upper and lower solution branches, the curves $\theta(\eta)$ vs. η of $\phi = 0.0$ remain higher than those of$\phi = 0.1$. Consequently, thermal radiation improves the nanofluid thermal diffusivity, i.e., for emergent values of radiation parameterN_R, heat will be supplemented to the regime and temperatures improved accordingly. As mentioned for heat transfer of flows over a stretching sheet, fluid temperature higher than both the wall temperature and the ambient temperature near the wall is

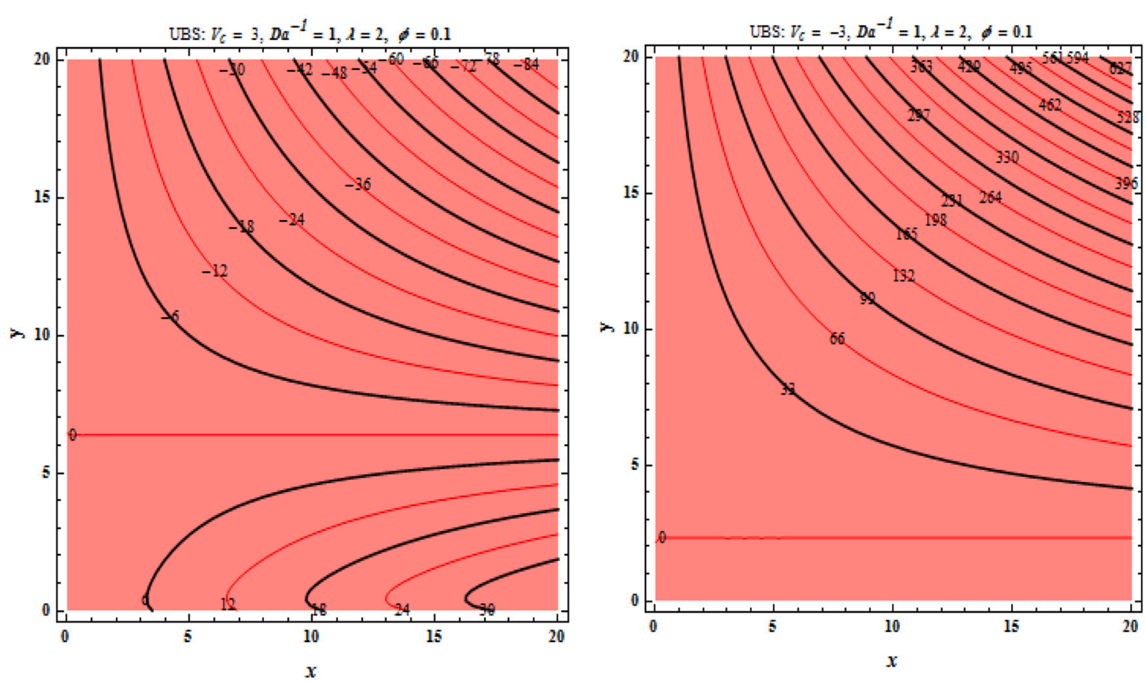

(a) (b)

Fig. 10. Plot showing of the stream function contour with (a) $V_c > 0$ (b)$V_c < 0$.

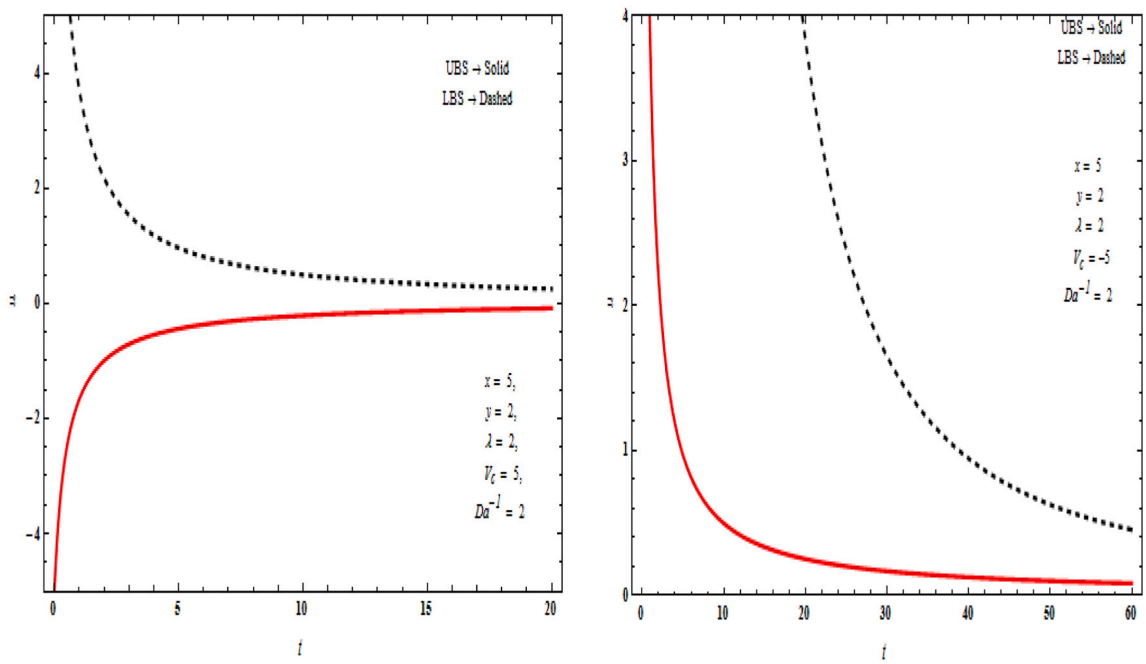

(a) (b)

Fig. 11. Axial and transverse velocity components for both branches (a) UBS (b) LBS.

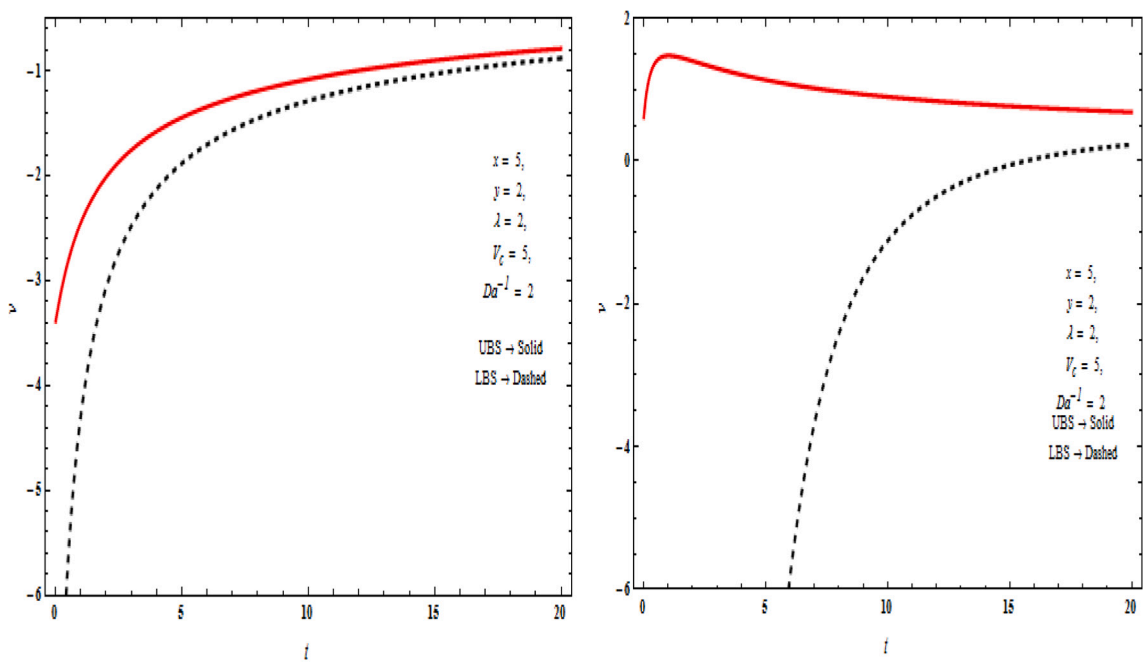

(a) (b)

Fig. 12. Axial and transverse velocity components for both branches (a) UBS (b) LBS.

physically achievable. Here we discuss of forced flow over a stretching sheet, we now look at heat transport in the presence of radiation. The effect of heat conductivity is amplified by the radiation. Radiation has the effect of dampening or enhancing heat transmission in a linear manner.As a result, thermal radiation enhances the thermal diffusivity of nanofluid, I.e., for rising quantities of radiation constraintN_R, heat will be improved in the system and temperatures will developed consequently. Fig. 7 depicts the temperature distribution $\theta(\eta)$ versus the similarity variable η for various values of the mass transpiration V_c with the stretching/shrinking surface. It is observed that the temperature $\theta(\eta)$ and boundary layer density rise in SWCNTs and MWCNTs. In the instance of mass transpiration V_c value rises as the temperature profile reduces. Fig. 8 depicts the temperature distribution $\theta(\eta)$ versus the similarity variable η for various values of the $Da^{-1}$with the stretching/shrinking surface.Fig. 9 depicts the temperature distribution $\theta(\eta)$ versus the similarity variable η for various values of the $Bi$with the stretching/shrinking surface. As a result, Biot number enhances the thermal diffusivity of nanofluid for rising quantities ofBi. The nanofluids are efficiency in the Bi as the temperature rises. The performance of nanofluids is affected by both the drop in particle volume fraction and the increase in temperature in the flow pattern.

Figs. 10a-b demonstrate the streamlined flow behavior for the two scenarios, suction as well as injection, correspondingly. We can plainly see the difference between streamline flows in both circumstances. The application of mass transpiration creates significant free flow, which causes the velocity boundary to flatten. Both situations of suction as well as injection.

Figs. 11a-b as well as Figs. 12a-b show the influence of axial and transverse velocities for litigation concerning injection as well as suction, respectively. It depicted an impact of Da^{-1}andV_c, respectively. As the velocity approaches zero in both situations, it is clear that wall stretching has no effect upon solution domain. For the lower branch solution, however, fluid passes along the axis and then constructively gradually decreases. Owing to reverse boundary layer processes, the transverse velocities for all divisions cease to zero at specific flow times, and it might be significant at other places for combined UBS and LBS.

4. Conclusions

The new classical results are illustrated by unsteady rear stagnation point flow of CNTs through porous media via stretching/shrinking boundary in the incidence of Darcy number, V_c, with N_R. The controlling PDEs are turned into ODEs consuming similarity variables, which are then explained analytically and expressed as an incomplete gamma function. Graphical visualisations can be used to determine the latest findings.

- The selection of moderating variables yields closed form accurate analytical answers for combined velocity and temperature.
- Various flows and heat transfer issues under mass transpiration and Darcy number may have two solution branches. Studies illustrate how the regulating variables have a serious impact on motion as well as heat exchange properties.
- When $Da^{-1} = N_R = 0$ and $B_i \to \infty$, the consequences are transformed into Fang et al. [32].
- $Da^{-1} = 0$ and $B_i \to \infty$, The data is then transformed into Mahabaleshwar et al. [33]

CRediT authorship contribution statement

U. S. Mahabaleshwar: Supervision, Conceptualization, Methodology, Formal analysis, Writing - original draft, review & editing.

K. N. Sneha: Conceptualization, Investigation, Methodology, Modeling, Writing - review & editing.

L. M. Pérez: Methodology, Writing - review & editing.

O. Manca: Supervision, Methodology, Writing - review & editing.

Declaration of Competing Interest

The authors declare that they have no known competing financial interests or personal relationships that could have appeared to influence the work reported in this paper.

Data availability

Data will be made available on request.

Acknowledgments

L.M.P. acknowledges financial support from ANID through Convocatoria Nacional Subvencion a Instalacion en la Academia Convocatoria Ano 2021. Also, Dr. U.S. Mahabaleshwar is thankful to University of Tarapaca, Chile hospitality during his stay and Università degli Studi della Campania "Luigi Vanvitelli", Italy.

References

[1] B.C. Sakiadis, Boundary-layer behavior on continuous solid surface, boundary layer equation for two-dimensional and axisymmetric flow, AICHE J. 7 (1961) 26, https://doi.org/10.1002/aic.690070108.

[2] L.J. Crane, Flow past a stretching plate, Z. Angew. Math. Mech. 21 (1970) 645–647, https://doi.org/10.1007/BF01587695.

[3] J.B. McLeod, K.R. Rajagopal, On the uniqueness of flow of a navier-stokes fluid due to a stretching boundary, Arch. Rat. Mech. An. 98 (1987) 385–393, https://doi.org/10.1007/BF00276915.

[4] P.S. Gupta, A.S. Gupta, Heat and mass transfer on a stretching sheet with suction and blowing, Can. J. Chem. Eng. 55 (1977) 744–746, https://doi.org/10.1002/cjce.5450550619.

[5] W.H.H. Banks, Similarity solutions of the boundary-layer equation for a stretching wall, J. Mech Theor. Appl. 13 (1988) 568–580.

[6] B.K. Dutta, P. Roy, A.S. Gupta, Temperature field in flow over a stretching sheet with uniform heat flux, Int. Comm. Heat Mass Transf. 12 (1985) 88–94, https://doi.org/10.1016/0735-1933(85)90010-7.

[7] M. Mahdavi, M. Sharifpur, J.P. Meyer, Fluid flow and heat transfer analysis of nanofluid jet cooling on a hot surface with various roughnesses, Int. Comm. Heat Mass Transf. 118 (2020), 104842, https://doi.org/10.1016/j.icheatmasstransfer.2020.104842.

[8] S.M. Murshed, M. Sharifpur, S. Giwa, J.P. Meyer, Experimental research and development on the natural convection of suspensions of nanoparticles, Nanomaterials 10 (2020) 1855, https://doi.org/10.3390/nano10091855.

[9] M. Sharifpur, N. Tshimanga, J.P. Meyer, O. Manca, Experimental investigation and model development for thermal conductivity of α-Al_2O_3-glycerol nanofluids, Int. Comm. Heat Mass Transf. 85 (2017) 12–22, https://doi.org/10.1016/j.icheatmasstransfer.2017.04.001.

[10] A. Brusly Solomon, M. Sharifpur, T. Ottermann, C. Grobler, M. Joubert, J.P. Meyer, Natural convection enhancement in a porous cavity with Al2O3-ethylene glycol/water nanofluids, Int. Comm. Heat Mass Transf. 108 (2017) 1324–1334, https://doi.org/10.1016/j.ijheatmasstransfer.2017.01.009.

[11] S. Reddy, A.J. Chamkha, Soret and Dufour effects on MHD convective flow of Al_2O_3–water and TiO_2–water nanofluids past a stretching sheet in porous media with heat generation/absorption, Adv. Powder Technol. 27 (2016) 1207–1218, https://doi.org/10.1016/j.apt.2016.04.005.

[12] R.S.R. Gorla, A. Chamkha, Natural convective boundary layer flow over a non isothermal vertical plate embedded in a porous medium saturated with a nanofluid, Nanoscale Microscale Thermophys. Eng. 15 (2011) 81–94, https://doi.org/10.1080/15567265.2010.549931.

[13] S. Iijima, Helical microtubules of graphitic carbon, Nature 354 (1991) 56–64, https://doi.org/10.1038/354056a0.

[14] L.W. Zhang, Z.X. Lei, K.M. Liew, Computation of vibration solution for functionally graded carbon nanotube-reinforced composite thick plates resting on elastic foundations using the element-free IMLS-Ritz method, Appl. Math. Comput. 256 (2015) 488–504, https://doi.org/10.1016/j.amc.2015.01.066.

[15] K. Kiani, Nanomechanical sensors based on elastically supported double-walled carbon nanotubes, Appl. Math. Comput. 270 (2015) 216–241, https://doi.org/10.1016/j.amc.2015.07.114.

[16] V. Kumaresan, R. Velraj, S.K. Das, Convective heat transfer characteristics of secondary refrigerant based CNT nanofluids in a tubular heat exchanger, Int. J. Refrig. 35 (2012) 2287–2296, https://doi.org/10.1016/j.ijrefrig.2012.08.009.

[17] Z.-H. Liu, L. Liao, Forced convective flow and heat transfer characteristics of aqueous drag-reducing fluid with carbon nanotubes added, Int. J. Them. Sci. 49 (2010) 2331–2338, https://doi.org/10.1016/j.ijthermalsci.2010.08.001.

[18] M.H. Ahmadi, A. Mirlohi, M. Alhuyi Nazari, R. Ghasempour, A review of thermal conductivity of various nanofluids, J. Mol. Liq. 265 (2018) 181–188, https://doi.org/10.1016/j.molliq.2018.05.124.

[19] A. Baghban, M. Kahani, M.A. Nazari, M.H. Ahmadi, W.-M. Yan, Sensitivity analysis and application of machine learning methods to predict the heat transfer performance of CNT/water nanofluid flows through coils, Int. J. Heat Mass Transf. 128 (2019) 825–835, https://doi.org/10.1016/j.ijheatmasstransfer.2018.09.041.

[20] R. Loni, E.A. Asli-Ardeh, B. Ghobadian, M.H. Ahmadi, E. Bellos, GMDH modeling and experimental investigation of thermal performance enhancement of hemispherical cavity receiver using MWCNT/oil nanofluid, Sol. Energy 171 (2018) 790–803, https://doi.org/10.1016/j.solener.2018.07.003.

[21] L.D. Gu, J.C. Min, Y.C. Tang, Effects of mass transfer on heat and mass transfer characteristics between water surface and airstream, Int. J. Heat Mass Transf. 222 (2018) 2093–2202, https://doi.org/10.1016/j.ijheatmasstransfer.2018.02.061.

[22] M.H. Esfe, A.A.A. Arani, M. Rezaie, W.-M. Yan, A. Karimipour, Experimental determination of thermal conductivity and dynamic viscosity of ag–MgO/water hybrid nanofluid, Int. Comm. Heat Mass Transf. 66 (2015) 189–195, https://doi.org/10.1016/j.icheatmasstransfer.2015.06.003.

[23] M. Astanina, M. Sheremet, U.S. Mahabaleshwar, J. Singh, Effect of porous medium and copper heat sink on cooling of heat-generating element, Energies 13 (2020) 2538, https://doi.org/10.3390/en13102538.
[24] J. Singh, U.S. Mahabaleshwar, G. Bognár, Mass transpiration in nonlinear MHD flow due to porous stretching sheet, Sci. Rep. 9 (2019) 18484, https://doi.org/10.1038/s41598-019-52597-5.
[25] T. Anusha, U.S. Mahabaleshwar, Y. Sheikhnejad, An MHD of nanofluid flow over a porous stretching/shrinking plate with mass transpiration and brinkman ratio, Trans. Porous Medium 142 (2022) 333–352, https://doi.org/10.1007/s11242-021-01695-y.
[26] U.S. Mahabaleshwar, T. Anusha, P.H. Sakanaka, S. Bhattacharyya, Impact of inclined Lorentz force and Schmidt number on chemically reactive Newtonian fluid flow on a stretchable surface when Stefan blowing and thermal radiation are significant, Arab. J. Sci. Eng. 46 (2021) 12427–12443, https://doi.org/10.1007/s13369-021-05976-y.
[27] U.S. Mahabaleshwar, K.N. Sneha, H.-N. Huang, An effect of MHD and radiation on CNTS-water based nanofluid due to a stretching sheet in a Newtonian fluid, Case Studies Thermal Eng. 28 (2021), 101462, https://doi.org/10.1016/j.csite.2021.101462.
[28] A. Mastroberardino, U.S. Mahabaleshwar, Mixed convection in viscoelastic flow due to a stretching sheet in a porous medium, J. Porous Media 16 (2013) 483–500, https://doi.org/10.1615/JPorMedia.v16.i6.10.
[29] D.A. Nield, The boundary correction for the Rayleigh-Darcy problem: limitations of the brinkman equation, J. Fluid Mech. 128 (1983) 37–46, https://doi.org/10.1017/S0022112083000361.
[30] S. Rosseland, Astrophysik and atomtheoretische Grundlagen, Springer-Verlag, Berlin, 1931.
[31] T. Fang, W. Jing, Closed-form analytical solutions of flow and heat transfer for an unsteady rear stagnation point flow, Int. J. Heat Mass Transf. 62 (2013) 55–62, https://doi.org/10.1016/j.ijheatmasstransfer.2013.02.049.
[32] M.A. Xenos, E.N. Petropoulou, A. Siokis, U.S. Mahabaleshwar, Solving the nonlinear boundary layer flow equations with pressure gradient and radiation, Symmetry 12 (2020) 710, https://doi.org/10.3390/sym12050710.
[33] U.S. Mahabaleshwar, K.R. Nagaraju, P.N. Vinay Kumar, M.N. Nadagouda, R. Bennacer, M.A. Sheremet, Effects of Dufour and Soret mechanisms on MHD mixed convective-radiative non-Newtonian liquid flow and heat transfer over a porous sheet, Therm. Sci. Eng. Prog. 16 (2020), 100459, https://doi.org/10.1016/j.tsep.2019.100459.
[34] K. Hiemenz, Grenzschicht an einem in den gleichformigenglussigkeitsstrom eingetauchten geraden kreiszylinder, Dinglers Polytechnisches J. 326 (1911) 321–410.
[35] H.G. JiLe, S. Qayyum, F. Shah, M.I. Khan, S.U. Khan, Slip flow of Jeffrey nanofluid with activation energy and entropy generation applications, Adv. Mech. Eng. 13 (3) (2021), https://doi.org/10.1177/16878140211006578.
[36] S. Ahmad, T. Hayat, A. Alsaedi, H. Ullah, F. Shah, Computational modeling and analysis for the effect of magnetic field on rotating stretched disk flow with heat transfer, Propul. Power Res. 10 (2021) 48–57, https://doi.org/10.1016/j.jppr.2020.11.005.
[37] T. Hayat, F. Shah, M.I. Khan, A. Alsaedi, T. Yasmeen, Modeling MHD stagnation point flow of thixotropic fluid with non-uniform heat absorption/generation, Microgravity Sci. Tech. 29 (2017) 459–465, https://doi.org/10.1007/s12217-017-9564-7.
[38] Y.-J. Xu, F. Shah, M.I. Khan, R. Naveen Kumar, R.J. Punith Gowda, B. C. Prasannakumara, M.Y. Malik, S.U. Khan, New modeling and analytical solution of fourth grade (non-Newtonian) fluid by a stretchable magnetized Riga device, Int. J. Modern Physics C 33 (2022) 2250013, https://doi.org/10.1142/S0129183122500139.
[39] T. Hayat, F. Shah, A. Alsaedi, B. Ahmad, Entropy optimized dissipative flow of effective Prandtl number with melting heat transport and joule heating, Int. Comm. Heat Mass Transf. 111 (2020), 104454, https://doi.org/10.1016/j.icheatmasstransfer.2019.104454.
[40] K. Muhammad, T. Hayat, A. Alsaedi, A comparative study for convective flow of basefluid (gasoline oil), nanomaterial (SWCNTs) and hybrid nanomaterial (SWCNTs + MWCNTs), Appl. Nanosci. 11 (2021) 9–20, https://doi.org/10.1007/s13204-020-01559-9.
[41] K. Muhammad, T. Hayat, A. Alsaedi, Numerical study of Newtonian heating in flow of hybrid nanofluid (SWCNTs + CuO + Ethylene glycol) past a curved surface with viscous dissipation, J. Therm. Anal. Calorim. 143 (2021) 1291–1302, https://doi.org/10.1007/s10973-020-10196-x.
[42] K. Muhammad, T. Hayat, A. Alsaedi, Mixed convective slip flow of hybrid nanofluid (MWCNTs + Cu + Water), nanofluid (MWCNTs + Water) and base fluid (Water): a comparative investigation, J. Therm. Anal. Calorim. 143 (2021) 1523–1536, https://doi.org/10.1007/s10973-020-09577-z.
[43] U.S. Mahabaleshwar, K.N. Sneha, A. Wakif, Significance of thermo-diffusion and chemical reaction on MHD Casson fluid flows conveying CNTs over a porous stretching sheet, Waves Random Complex Media (2023), https://doi.org/10.1080/17455030.2023.2173500.
[44] U.S. Mahabaleshwar, K.N. Sneha, A. Miyara, M. Hatami, Radiation effect on inclined MHD flow past a super-linear stretching/shrinking sheet including CNTs, Waves Random Complex Media (2022), https://doi.org/10.1080/17455030.2022.2053238.
[45] K.N. Sneha, U.S. Mahabaleshwar, A. Chan, M. Hatami, Investigation of radiation and MHD on non-Newtonian fluid flow over a stretching/shrinking sheet with CNTs and mass transpiration, Waves Random Complex Media (2022), https://doi.org/10.1080/17455030.2022.2029616.
[46] T.G. Fang, F.J. Wang, B. Gao, Unsteady magnetohydrodynamic stagnation point flow closed-form analytical solutions, Appl. Math. Mech. 40 (4) (2019) 449–464, https://doi.org/10.1007/s10483-019-2463-7.
[47] A.B. Vishalakshi, U.S. Mahabaleshwar, G. Lorenzini, An unsteady Hiemenz stagnation point flow of MHD Casson nanofluid due to a superlinear stretching/shrinking sheet with heat transfer, J. Adv. Res. Flud. Mech. Therm. Sci. 95 (2022) 1–19.

Update

International Communications in Heat and Mass Transfer
Volume 146, Issue , July 2023, Page

DOI: https://doi.org/10.1016/j.icheatmasstransfer.2023.106926

International Communications in Heat and Mass Transfer 146 (2023) 106926

Contents lists available at ScienceDirect

International Communications in Heat and Mass Transfer

journal homepage: www.elsevier.com/locate/ichmt

Corrigendum to "An unsteady flow through porous media leads to a Newtonian fluid presence of CNTS and suction/injection" [International Communications in Heat and Mass Transfer 145 (2023) 106844]

U.S. Mahabaleshwar [a], K.N. Sneha [a], L.M. P'erez [b], O. Manca [c,*]

[a] Department of Studies in Mathematics, Davangere University, Shivagangothri, Davangere 577 007, India
[b] Departamento de Física, FACI, Universidad de Tarapaca, Casilla 7D, Arica, Chile
[c] Dipartimento di Ingegneria, Universit`a degli Studi della Campania Luigi Vanvitelli, Aversa, CE, Italy

In Acknowledgments

Errata:

"L.M.P. acknowledges financial support from ANID through Convocatoria Nacional Subvencion a Instalacion en la Academia Convocatoria Ano 2021. Also, Dr. U.S. Mahabaleshwar is thankful to University of Tarapaca, Chile hospitality during his stay and Università degli Studi della Campania 'Luigi Vanvitelli', Italy."

Corrige:

"L.M.P. acknowledges financial support from ANID through Convocatoria Nacional Subvencion a Instalacion en la Academia Convocatoria Ano 2021, Grant SA77210040. Also, Dr. U.S. Mahabaleshwar is thankful to University of Tarapaca, Chile hospitality during his stay and Università degli Studi della Campania 'Luigi Vanvitelli', Italy."

DOI of original article: https://doi.org/10.1016/j.icheatmasstransfer.2023.106844.

* Corresponding author.
E-mail address: oronzio.manca@unicampania.it (O. Manca).

https://doi.org/10.1016/j.icheatmasstransfer.2023.106926

Available online 4 July 2023